

CHROMOSPHERIC K CaII TELESCOPE OF BAIKAL ASTROPHYSICAL OBSERVATORY. NEW LIGHT

L.S. Lopteva

*Institute of Solar-Terrestrial Physics SB RAS,
Irkutsk, Russia, lopteva@iszf.irk.ru*

G.I. Kushtal

*Institute of Solar-Terrestrial Physics SB RAS,
Irkutsk, Russia, kushtal@iszf.irk.ru*

V.A. Proshin

*Institute of Solar-Terrestrial Physics SB RAS,
Irkutsk, Russia, pro@iszf.irk.ru*

V.I. Skomorovsky

*Institute of Solar-Terrestrial Physics SB RAS,
Irkutsk, Russia, skoal@iszf.irk.ru*

S.V. Firstov

*Institute of Solar-Terrestrial Physics SB RAS,
Irkutsk, Russia, firstov@mail.ru*

V.A. Khimich

*Institute of Solar-Terrestrial Physics SB RAS,
Irkutsk, Russia, khimval@mail.ru*

S.A. Chuprakov

*Institute of Solar-Terrestrial Physics SB RAS,
Irkutsk, Russia, chupr@iszf.irk.ru*

Abstract. In recent years, most results of CaII studies of the solar chromosphere in H and K lines have been based on observations with narrow passband filters. The Baikal Observatory's full-disk chromospheric telescope for the K CaII line with a birefringent filter (BF) has again been included in observation programs of the Sun Service Station and scientific research.

We analyze the methods of telescope and modernized birefringent filter adjustment. After many years of continuous operation, a pressing need arose to replace the damaged parts of the chromospheric telescope. Optics and mechanics of the entire telescope have been cleaned and readjusted. Wavefront interferograms of the teleobjective lens and of the whole telescope show that wavefront distortions of the entire optical path are within 0.25λ . We present an optical scheme and discuss

optical-physical characteristics of BF elements. The interference prefilter and UV polarizers have been replaced, and passbands of BF tunable stages have been adjusted. The BF spectral characteristics provide a fairly high contrast of monochromatic images of large-scale phenomena. Unfortunately, with a collimator and Sony Cyber-Shot DSC-S85 camera, mounted on the telescope, the theoretical resolution of the 180 mm telescope is not realized. We have therefore calculated two optical schemes of telescope changes for possible improvement in spatial resolution.

Keywords: chromospheric telescope, birefringent filter, interferometric measurements.

INTRODUCTION

More than 25 years ago, the Institute of Solar-Terrestrial Physics (SibIZMIR) designed and built a telescope for regular full-disk observations of the chromosphere with a birefringent filter (BF) for the K CaII line ($\lambda=3934 \text{ \AA}$). The chromospheric telescope is installed in the Baikal Astrophysical Observatory (BAO) near the village of Listvyanka on the west coast of Lake Baikal. At present, some observation problems crucial for the development of the telescope [Trifonov et al., 1992] have already been solved, but on the whole the problems that require observations in the K CaII line remain unsolved. Recent observations in new spectral regions (UV, X-ray, and radio range) for their correct interpretation need to be compared with familiar observations in the K CaII and H α lines. The nature of the spatial coherence of the magnetic field fine structure has not been determined yet, and K CaII observations provide additional information for direct measurements of the magnetic field vector with high temporal resolution. The K CaII filtergrams are still effective in studies of solar polar regions.

Calculation of optics, its manufacture, design of the telescope mechanics, construction of the tower, and installation of the telescope in it were fully implemented at ISTP SB RAS in 1991–1992.

Full-disk observations of the chromosphere in the K CaII line have been performed at BAO since 1992. In the first decade, 50 mm solar images were taken by an 80 mm camera [Trifonov et al., 1992]. In 2003, when passing from photographic to electronic image registration with the Sony Cyber-Shot DSC-S85 camera, the optical scheme of the telescope was changed [Trifonov et al., 2004], and the last maintenance and adjustment of the telescope were carried out. Over 14 years of follow-up operation, the telescope's optics became dirty, barrels got rusty, some mechanical control assemblies got worn out. Alignment of the telescope's optics and BF deteriorated, and the most important thing is that contrast and sharpness of the image, on which an image with a strange structure was sometimes superimposed, decreased.

The telescope's optics was completely disassembled, cleared, and adjusted, new polarization elements were installed, and the BF passband was tuned.

DESCRIPTION OF THE TELESCOPE

The telescope and its optical scheme after modernization in 2003 [Trifonov et al., 2004] are shown in Figure 1. The teleobjective (positive and negative lenses) and field lens produce a primary solar image 20 mm in diameter in the telecentric beam path inside BF. Characteristics of the telescope and BF are listed in Table. One of the conditions for successful operation of the telescope-filter complex is the compliance of its optical scheme for image construction with the following requirements on the BF installation: preserving irradiance monochromaticity for given parameters of the filter and providing the desired resolution over the entire solar disk [Klevtsov, 1984]. BF parameters: the length of the BF optical stack is 217 mm, its clear aperture is 30 mm, its angular field of view is $\pm 2.5^\circ$ (with allowable shift of passband maximum within 0.06 \AA for oblique beams). These very parameters and the size of the non-vignetted field of view of $34'$ exceeding the Sun's angular diameter determined the maximum allowable lens diameter for the telescope — no more than 180 mm [Klevtsov, 1984]. Next to BF is a collimator ($F=170 \text{ mm}$) which forms an image of the entrance pupil in its focus on the lens of the digital camera Sony Cyber-Shot DSC-S85; and in front of BF, a virtual solar image recorded with the camera.

BF

K CaII $\lambda 3934 \text{ \AA}$ BF manufactured by Bernhard Halle Nachfl. GmbH was received by ISTP SB RAS in 1969. The nominal full width at half maximum (FWHM) is 0.3, 0.6, or 1.2 \AA . The 0.3 \AA passband can be shifted within $\pm 0.3 \text{ \AA}$ by rotating the entrance and exit polarizers through gear train – line-shifter. The filter was utilized in spectral observations of the fine structure of the solar chromosphere as a photographic guide on the horizontal telescope ATSU-5 of the Sayan Solar Observatory to photograph an area of the solar image reflected from jaws of the spectrograph mirror slit.

This filter was intended to be used for calculating optics of the full-disk chromospheric telescope in the K CaII line. Figure 2 is a schematic of the filter optical stack and the structure of polarization stages. BF has ten polarization stages composed of Iceland spar and quartz crystal plates installed between seven polarizers. Five stages with high-order interference are wide-angle (the first-type Lyot scheme with half-wave plates), four stages are split according to the Evans scheme [Evans, 1949] in order to decrease the number of polarizers absorbing light in the UV spectral region in which to reduce light losses five birefringent prisms (spar-fused quartz) are utilized as polarizers within the stack. The prisms transmit an extraordinary beam without deflection and deflect an ordinary beam by 6.3° .

Characteristics of the telescope and BF

Telescope	
Clear aperture of the lens	180 mm
Equivalent focal distance teleobjective + field lens	2147.5 mm
Non-vignetted field of view	$34'$
Theoretical spatial resolution	$0.55''$
BF	
K CaII FWHM	0.54 \AA
Angular field of view	$\pm 2.5^\circ$
Clear aperture of crystal stack	30 mm
Spectral shift of the passband position	$\pm 0.3 \text{ \AA}$

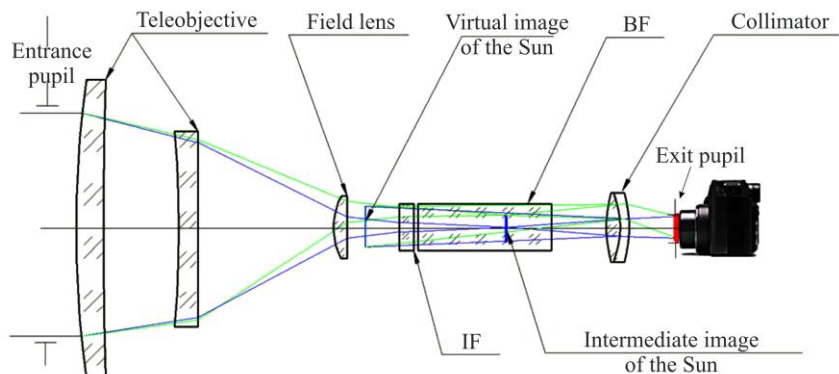


Figure 1. Telescope and its optical scheme after modernization in 2003 [Trifonov, 2004]

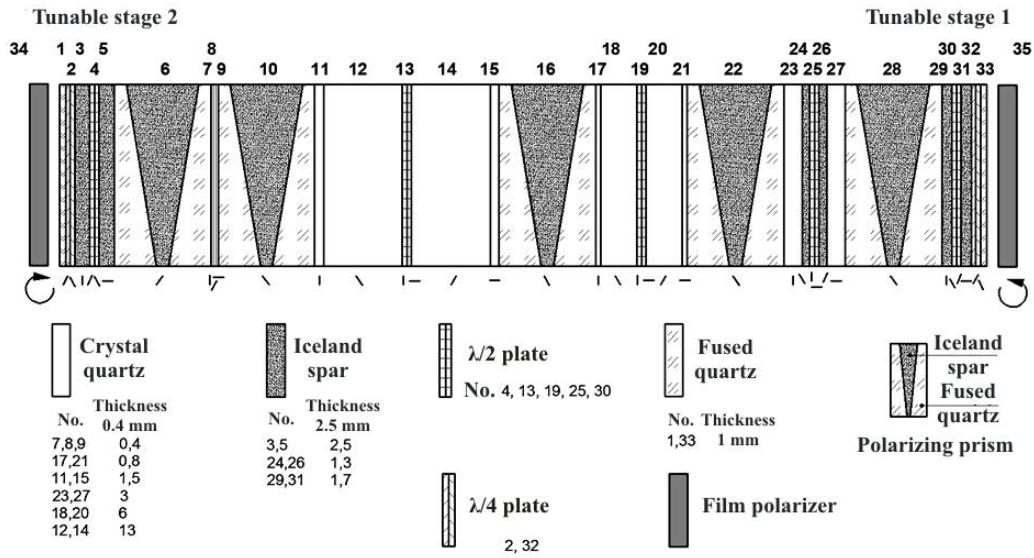


Figure 2. Scheme of the BF optical stack for the K CaII line (Bernhard Halle Nachfl. GmbH)

Figure 3 shows five polarization prisms disassembled: the central part includes 5 isosceles prisms made of Iceland spar and 10 right-angle lateral prisms made of fused quartz. The photos were taken during the repair of Kislovodsk station's BF. Prisms of this filter of earlier production were glued with optical cement. Owing to the contact of immersion by which adjacent crystal plates were assembled with the cement layer, the prisms became blurred and lost their transparency. The prisms of BF of later production were assembled by immersion.

The scattered light produced by the beams deflected by prisms and reflected from the lateral surface of the optical stack is trapped by diaphragms (sawcuts at the base of prisms of Iceland spar) and annular diaphragms (blackened steps on the periphery of right-angle prisms). The entire stack is assembled by immersion in a cylindrical tube and protected by fused-quartz glasses. Two external wide-angle stages made of highest-order interference Iceland spar are tunable and comprise quarter-wave plates behind which outside the stack film polarizers 34, 35 are installed (Figure 2). With the aid of the line-shifter the polarizers can be synchronously rotated for spectral tuning of the passband along the K CaII line profile.

The filter passband spectra obtained with the ASP-20 spectrograph of the ATSU-5 solar telescope in 1991 [Trifonov et al., 1992] showed that with FWHM of 0.3 Å the main filter passband, especially when shifted, has strong side lobes, which can reduce image contrast. A similar B. Halle BF for the K CaII line has been studied by Sotnikova [1977] "...for the narrowest passband of 0.3 Å as the most effective for observing chromospheric formations. The results showed that this filter can be applied to observations for shifts in line wings within ± 0.3 Å. At a shift by ± 0.4 Å, the intensity of side lobes greatly increases, and at a shift by ± 0.6 Å there appear two equally strong sidelobes spaced by 1.2 Å".

Spectral observations of solar plages in the 90s as well as areas in the quietest regions of the solar surface — supergranulation cells — have revealed that the distance between calcium line self-reversal peaks K_{2V} and K_{2R} is, on average, within 0.5–0.7 Å. The characteristic formations in the line are expectedly observed with the highest contrast if FWHM is 0.6 Å with a ± 0.3 Å passband shift (R.B. Teplitskaya, private communication).

It has therefore been decided to increase the passband contrast before installing the filter in the chromospheric telescope — without fundamental change in the



Figure 3. Birefringent prisms of BF: central components (left); lateral components (right)

scheme, FWHM was left 0.6 \AA and side lobes were reduced using the contrast polarization stage. In the BF stack (Figure 2), thicknesses of the Iceland spar and quartz crystal plates of all stages, except for plates of tunable stages of Iceland spar 3, 5 and 27, 29, correspond to the B. Halle scheme. To extend the passband, the 5.029 mm plates of elements 3 and 5 were removed from the scheme and replaced by 2.515 mm plates of elements 27, 29 of the same stack. To increase the contrast (suppress the nearest side lobes), new plates 1.746 mm thick (not multiple of 2) were designed, manufactured, and installed in elements 27 and 29. Accordingly, in the line-shifter instead of transmission 2:1 transmission 1.44:1 proportional to the ratio between thicknesses of plates is installed for a concordant shift of the passband of these stages by rotating the external polarizers.

RECONSTRUCTION OF THE TELESCOPE IN 2018

Despite the relatively clear Baikal atmosphere, over the 14-year all-year-round operation of the telescope's optics has been covered with dust coming from the nearest building constructions and with soot from forest fires. The front surface of the positive lens of the teleobjective was especially damaged. Due to accidental exposure to rain and moisture from patchy fogs, barrels got rusty. From three unloading spacers glued to the glass, diffuse spots spread over the surface of the negative lenses

(Figure 4). The main problem of the telescope is a decrease in contrast and sharpness of the solar image, which is sometimes superimposed by an unclear striped pattern (Figure 5). This might have been caused by defects in the BF stack in the prefilter. Owing to the tilt and decentering of BF, ordinary beams deflected by birefringent prisms might have entered the pupil of the lens of the Sony digital camera. The camera pupil was also found to be not optimally matched in size and position with the exit pupil of the telescope.

The work on improvement of image quality involved several stages. To identify causes of the defects, we examined optical and physical characteristics of the telescope and BF. Optical elements of BF and prefilter were replaced. We experimentally found the position of the entrance pupil of the camera and calculated parameters of the reimaging lens to optimize camera alignment. The teleobjective and other optics were completely disassembled and cleaned. The telescope was adjusted, interferometric measurements of the wavefront of the telescope were carried out and compared with calculated data.

BF modernization

The filter disassembly showed that in the optical stack of BF the film polarizers placed outside the optical stack have been put out of operation after the long period of observations. Affected by heating in the thermostat (the



Figure 4. Positive and negative teleobjective lenses

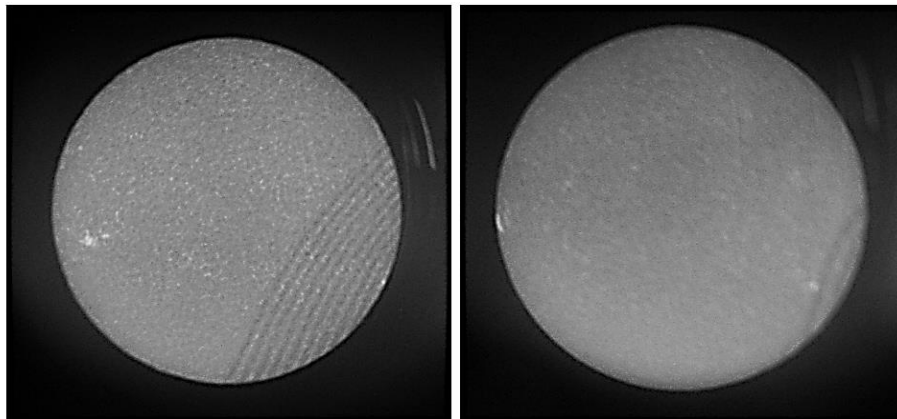


Figure 5. Defects of chromospheric telescope images

working temperature of the filter is ~45 °C) and in the solar beam, the stretched dichroic polaroid film, glued in protective glasses of fused quartz, shrunk. The effective work field became less than 10 mm. Furthermore, immersion by which the optical stack is assembled, evaporated and condensed on the polarizer surface facing the optical stack (Figure 6). The polarizers needed to be replaced with more effective ones.

The polarizer effectiveness is evaluated from basic characteristics of the polaroid film — maximum k_1 and minimum k_2 transmission coefficients of the linear-polarized light whose electric vector is directed respectively parallel and perpendicular to the stretch forming of the film. Then the polarizing ability or polarization effect (PE)

$$PE = \frac{k_1 - k_2}{k_1 + k_2} 100 \%,$$

where k_1 and k_2 are estimated relative to 100 % of polarized light.

The only manufacturer of polarizing films and polarizing light filters in Russia is Zagorsk Optical and Mechanical Plant. The plant currently has a pilot production line for manufacturing polarizing films and light filters for visible and IR spectral regions. However, these polarizers in the 3900 Å spectral region have low efficiency. Film polarizers in the spectral range 3900–10000 Å with high transmittance, efficiency, and uniformity are required not only to repair existing BF, but also to develop new BF to study the fine structure, magnetic fields, and velocities in the solar atmosphere. Transparency of polarizers is the determining factor in BF transmittance. Transparency requirements increase for the narrow filter passband, especially in the UV spectral region. To improve the BF transparency, as we can see in the case of the K CaII BF, crystalline prisms of Iceland spar are utilized as polarizers. However, the cost of such devices rises significantly.



Figure 6. Condensed oil on the surface of the external polarizer, placed after the prefilter before the BF stack. The polarizer is rotated using the line-shifter to shift the passband. Its barrel is linked with the limb, which in Angstrom units indicates the position of the BF passband relative to the line center

In cooperation of Open Joint Stock Company S.I. Vavilov State Optical Institute and Leningrad Optical Mechanical Association [Studying ..., 1984], possibilities of increasing the transmittance of dichroic polarizing films were explored for the visible spectral region by means of temperature/humidity processing and dosing irradiation. Fortunately, ISTP SB RAS has sample polaroid films with increased transmittance in the near-UV spectral region, which have been given for testing. These samples were installed instead of faded polaroid films between protective fused quartz glasses glued with the acrylic adhesive sufficiently transparent in the blue spectral region.

Figure 7 shows spectral characteristics of the old and new polarizers.

For the old B. Halle polarizer $k_1=0.58$ and $k_2=0.004$, and for the new one $k_1=0.72$ and $k_2=0.0055$. The polarizers have almost the same efficiency of ~0.98.

Spectral characteristics of the K CaII BF after assembly of the optical stack with new polarizers were obtained with a laboratory autocollimation spectrograph ($F=6$ m, the aperture ratio is 1:30, the grating is 300×200 mm, 600 groove/mm). The filter was set in the parallel beam; spectra were recorded by the linear CCD array (MORS). Passbands of tunable stages 1, 2 (Figure 8)

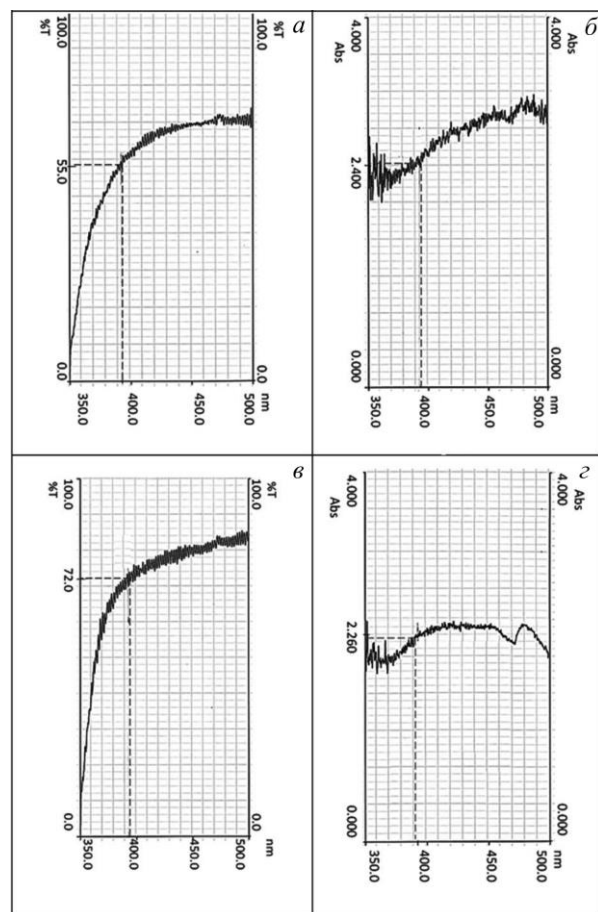


Figure 7. Spectra of transmission and optical density of the polarizers installed parallel and perpendicular to the transmission plane of the Glan-Thompson prism: old polarizer (a, b); new polarizer (c, d). The spectra were obtained with the spectrophotometer Hitachi U-3400 (Hitachi Ltd., Japan)

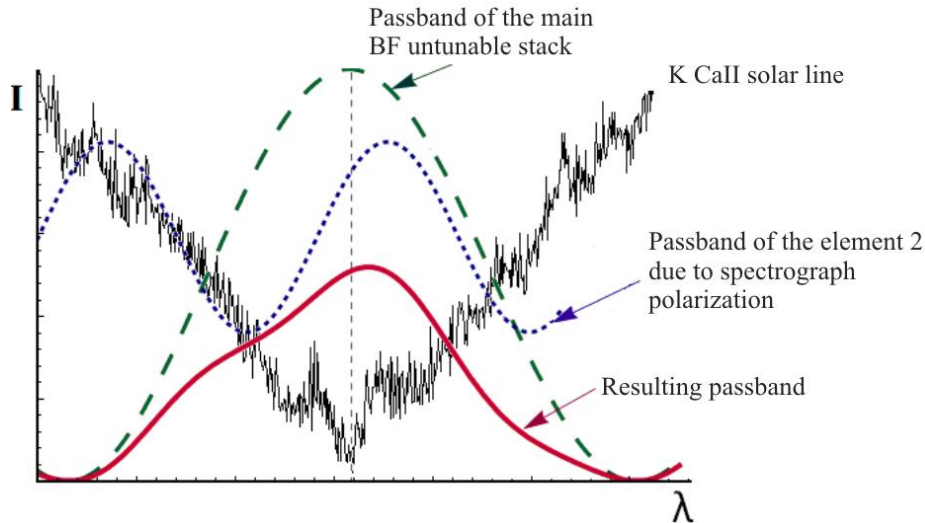


Figure 8. Distortion of the main BF stack passband due to light polarization in the spectrograph

were aligned with the passband of the main optical stack, taking into account that the light source — incandescent lamp — practically does not polarize light, whereas the spectrograph is a partial polarizer.

When tuning the maximum transmission of the main stack for the K CaII spectral line, external polarizers 34, 35 (see Figure 2) should be removed from the beam to make tunable stages 1 and 2 (Figure 2 and 9) ineffective — non-distorting the passband of the main stack. However, due to the partial light polarization by the diffraction grating of the spectrograph, the element of stage 2 modulates the passband of the main stack (Figure 8), and the resulting passband becomes asymmetric. This does not allow us to optimally tune the passband of the main stack to the K CaII line center through a change in temperature of the filter. To eliminate the effect of the spectrograph polarization, it is necessary to make element 2 ineffective. In the beam before the spectrograph slit (Figure 9), an additional quarter-wave plate and a polarizer (Glan-Thompson prism) are installed. The goal is to orient the additional quarter-wave plate perpendicular to the quarter-wave plate of the main stack (put plates for subtraction of birefringence), and to set the polarizer parallel to the optical axis of birefringent element 2 to exclude birefringence of the latter. The orientation of the quarter-wave plate of the optical stack of the filter is not visible from outside, so the additional polarizer and plate are sequentially rotated until modulation of the main stack passband disappears. By changing temperature, we tune the main stack to the K CaII line. Then, polarizer 35 of stage 1 is put into operation; by rotating the polarizer, the passband of the element of the stage is centered in the main stack passband profile. Then, the Glan-Thompson prism and additional quarter-wave plate are removed from the beam, polarizer 34 is put, and through its rotation the passband of the element of stage 2 is adjusted.

Spectra of the filter passband at a distance of 0, -0.18 , -0.32 , -0.48 , $+0.19$, $+0.35$, $+0.51$ Å from the center of the K CaII line at an operating temperature of 43.3 °C are shown in Figure 10. FWHM of the filter pass-

band in the line center is 0.54 Å. Transmission in line wings is normalized relative to the transmission at the center. When the passband is shifted to the red and blue spectral regions, transmittance of the filter should decrease, but this is not the case because of the asymmetry of the main stack profile caused by inaccurate birefringent elements manufactured by B. Halle.

The prefilter cuts adjacent main peaks of the optical stack transmission and prevents BF from overheating in the solar beam. It usually comprises a narrowband interference filter (IF) for operating wavelength, heat filter, and colored cutting-off glasses.

With time and when exposed to heat in the solar beam, the maximum transmission of this filter shifted from the central wavelength and the transmission decreased to 17 %. The passband of the new (2018) prefilter, made at ISTP SB RAS, is shown in Figure 11, *a*. FWHM is 38 Å, the bandwidth at a transmission level of 0.1 % is 156 Å. Transmission in λ 3933 Å is 24.6 %. The filter comprises two dielectric filters: narrowband contrast filter with 38 Å FWHM and heat filter cutting wings of the contrast filter up to 6000 Å (Figure 11, *b*—their common transmission). To cut IR spectral regions, colored glasses SZS-20 and FS-6 are installed (see Figure 11, *c*).

The joint transmission of BF and IF is ~ 5 – 7 %.

Adjustment and testing of the telescope's optics

In the original calculated optical scheme of the telescope [Trifonov et al., 1992], a solar image was formed by the reimaging lens on film of a camera. With the transition to the digital image recording in 2003, the reimaging lens was replaced by another, selected from the available ones.

This lens-collimator produces an image of the telescope pupil in the plane of the entrance pupil of the Sony digital camera lens. The lack of exact optical parameters of the collimator and Sony camera lens did not allow us to calculate and check their one-to-one correspondence and position when the camera was installed in 2003. It was tested and experimentally found in 2017 (see below).

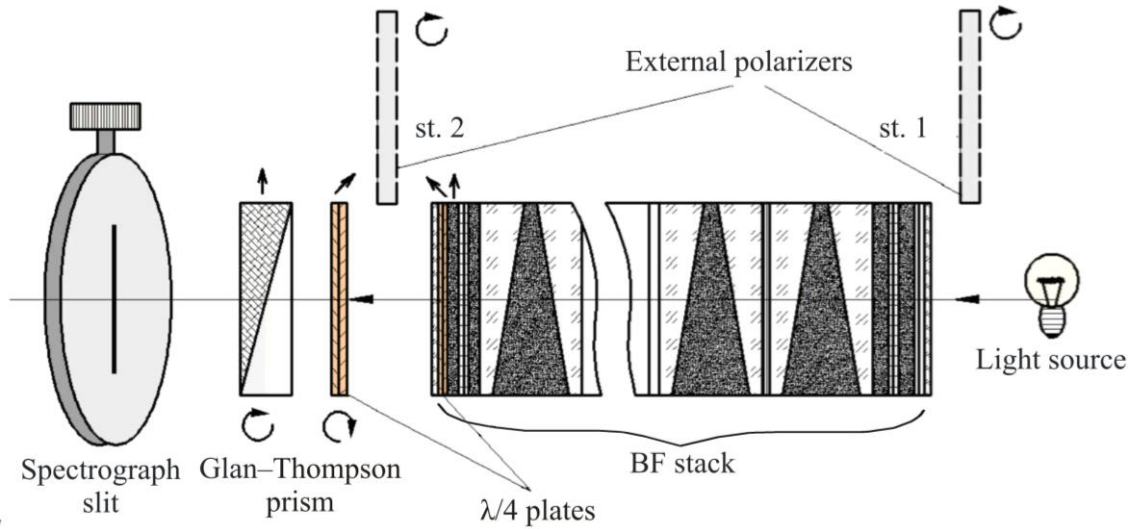


Figure 9. Scheme of BF passband tuning. Modulation of the passband of the main stack by the tunable element of stage 2 due to partial polarization in the spectrograph is eliminated when the axis of the rotated prism and additional $\lambda/4$ plate take the position indicated by upper arrows

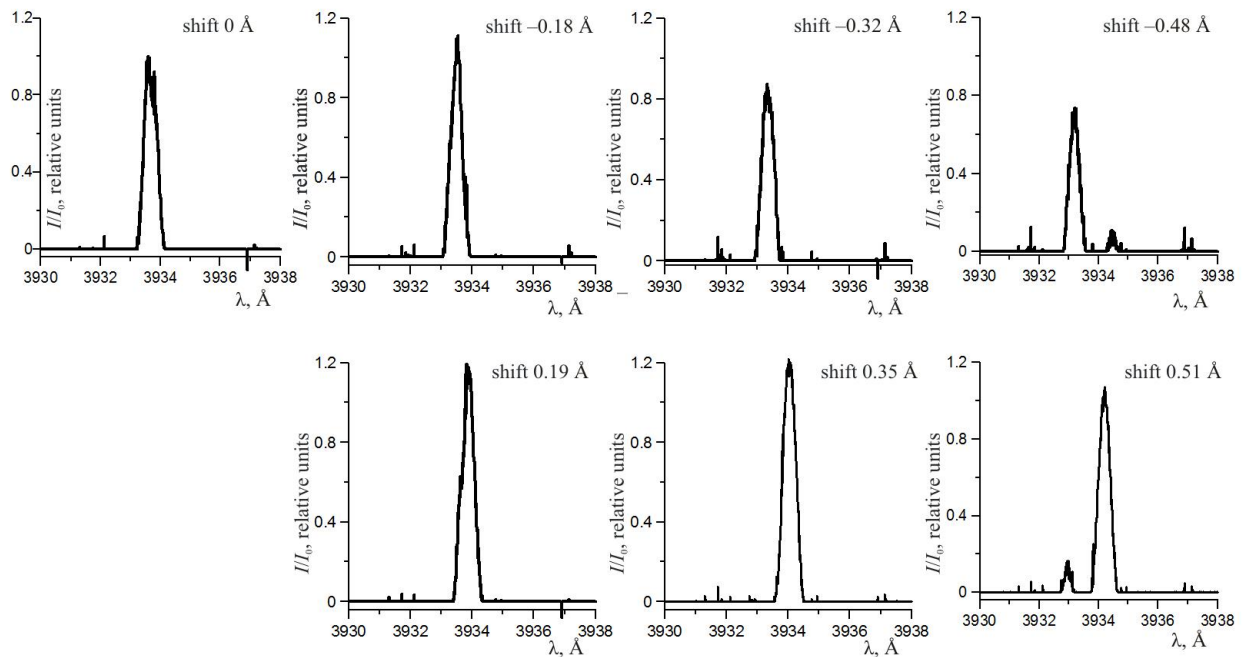


Figure 10. Profiles of BF passband in the line center and wings

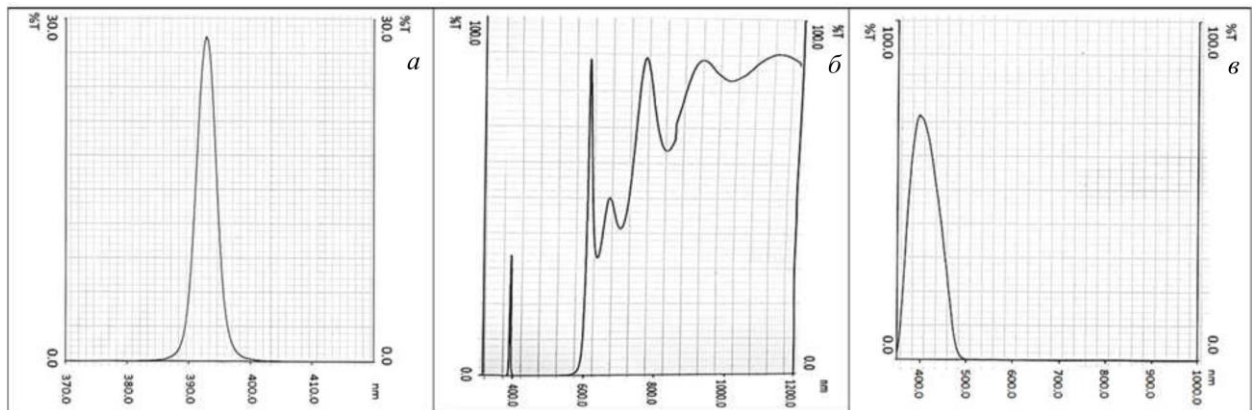


Figure 11. Profiles of prefilter passband and its components. Assembled in 2018

The telescope was reassembled and readjusted after its optics and mechanics had been thoroughly cleaned. The telescope optics was adjusted on an optical bench in laboratory setting at ISTP SB RAS. Skomorovsky et al. [2016] have described in detail the adjustment of a similar H α telescope.

The teleobjective (positive and negative lenses) in its barrel, field lens, BF, and collimator are successively arranged in the telescope tube consisting of sections (see Figure 1). All the optical elements have independent adjustments. The tilt and shift, beginning with the teleobjective and ending with the camera, are adjusted one-by-one using a laser mounted in front of the teleobjective behind the screen with a hole. On barrels of the teleobjective lenses, diaphragms with a 1–2 mm aperture are set up. A laser beam passes through the aperture in the screen and diaphragm. Using reflection glares from surfaces of the positive lens, first we eliminate the tilt of the external barrel of the teleobjective. Through transverse displacement and tilt of the negative lens, this glare is aligned with glares from its surfaces until a system of Newton interference rings, used for final adjustment of the teleobjective, appears. The teleobjective wavefront pattern (Figure 12) is recorded in the autocollimation scheme with the aid of a flat etalon and unequal-arm interferometer. After the teleobjective, the field lens is installed in the system and is adjusted. The teleobjective and field lens form an intermediate solar image in the telecentric beam path at an equivalent focal length of ~ 2 m (see Figure 1). In this focus, an interferometer is set and an image of the wavefront of the assembly of the teleobjective with field lens is obtained (Figure 13).

The comparison between wavefront interferograms of the teleobjective before its disassembly and after the new assembly and adjustment (see Figure 12, *a*, *b*) shows that the wavefront got better — in the old assembly the teleobjective was misaligned. After the new adjustment, the wavefront is consistent with the wavefront calculated using the Zemax program for a red laser wavelength of 6328 Å in the double beam path (Figures 12, *c*, 13, *c*). Due to the absence of a coherent light source with a wavelength of the K CaII line (λ 3933 Å), wavefront interferograms in this wavelength for assembling three telescope lenses were simulated only in Zemax (Figures 12, *d*, 13, *d*).

Wavefront distortions in the studied system for an axial point is 0.16λ for λ 3933 Å and are within the Rayleigh criterion.

BF is set in the telescope tube at the dovetail mount having adjustable movements — transverse displacement and tilt. The following requirements are imposed on the BF adjustment: a laser beam should pass through the center of optical windows of the filter with an accuracy 1–2 mm and deflect from the position of autocollimation by not more than 5'.

The collimator, which in its focus forms the entrance pupil of the telescope, is installed in the optical system in the last turn. Since in BF there are birefringent polarizing prisms, which permit an extraordinary beam to

pass without deflection and successively deflect an ordinary beam by $\sim 6.3^\circ$, at the output from the collimator there is a system of spaced-apart exit pupils. The scheme uses an undeflected pupil. The size of the exit pupil image and its position depend on parameters of the collimator. In 2003, a glued two-lens collimator ($F=170$ mm), which was not made at the ISTP SB RAS laboratory, was installed in the scheme. There was no information on its optical parameters required to calculate the whole scheme of the telescope. The wavefront error of the collimator, as measured in a parallel beam with the Twyman interferometer, is $N\sim 0.5$. The collimator forms an image of the entrance pupil of the telescope at the lens of the digital camera Sony Cyber-Shot DSC-S85 with parameters: 1704×2272 pixel matrix (5.358×7.144 mm), Carl Zeiss lens, $7\div 21$ mm focal length, and f-number $F2.0\div F2.5$ for $1^X\div 3^X$ zoom. As discussed, we could not find an optical scheme of this lens, and therefore it was unclear whether the entrance pupil was in the correct position relative to the exit pupil of the telescope. The correct position was found from the experiment, not from calculations.

Alignment of the telescope's exit pupil with the camera's entrance pupil

The focal length of the collimator of the telescope defines the size and position of the exit pupil of the telescope and the size of an image taken by the camera. With the 180 mm entrance aperture of the telescope, the collimator with the focus $f=170$ mm forms a 14.4 mm exit pupil. The calculated size of the entrance pupil of the Sony camera lens, placed behind the collimator, is dictated by the technical data sheet of the camera. When changing zoom from 1^X to 3^X , the aperture number varies from $F2$ (7 mm focal length) to $F2.5$ (21 mm focal length). The pupil size increases from 3.5 to 8.4 mm. The telescope uses the full aperture, if the exit pupil of the telescope is aligned with the entrance pupil of the camera in position along the optical axis and in size. If the pupils are aligned in position with the 8.4 mm pupil of the camera, the central 130 mm teleobjective zone is effective (Figure 14, *a*), and its entire external zone up to the diameter of 180 mm does not work, with the theoretical resolution of the telescope being not higher than 1.1". If the pupils are misaligned, irradiance from the teleobjective zone beyond the 130 mm diameter falls into the pupil and the zone expands with the pupils spaced apart, whereas irradiance from the zones within the 130 mm diameter is trapped by the camera pupil (Figure 14, *b*).

The mutual position of the camera's entrance pupil and the telescope's exit pupil and the actual size of the camera's entrance pupil for two magnifications were determined on the optical bench, where the wavefront was explored and the telescope was adjusted. An artificial sun for the telescope was simulated using the autocollimator OSK-2 with a 150 mm lens and a 1600 mm focal length (Figure 15).

In the OSK-2 focus, the "sun" was put — a transparent circle of size 14.8 mm. An illuminator is an incan-

descent lamp, ground glass, light filter for the blue spectral region. When working with the artificial sun,

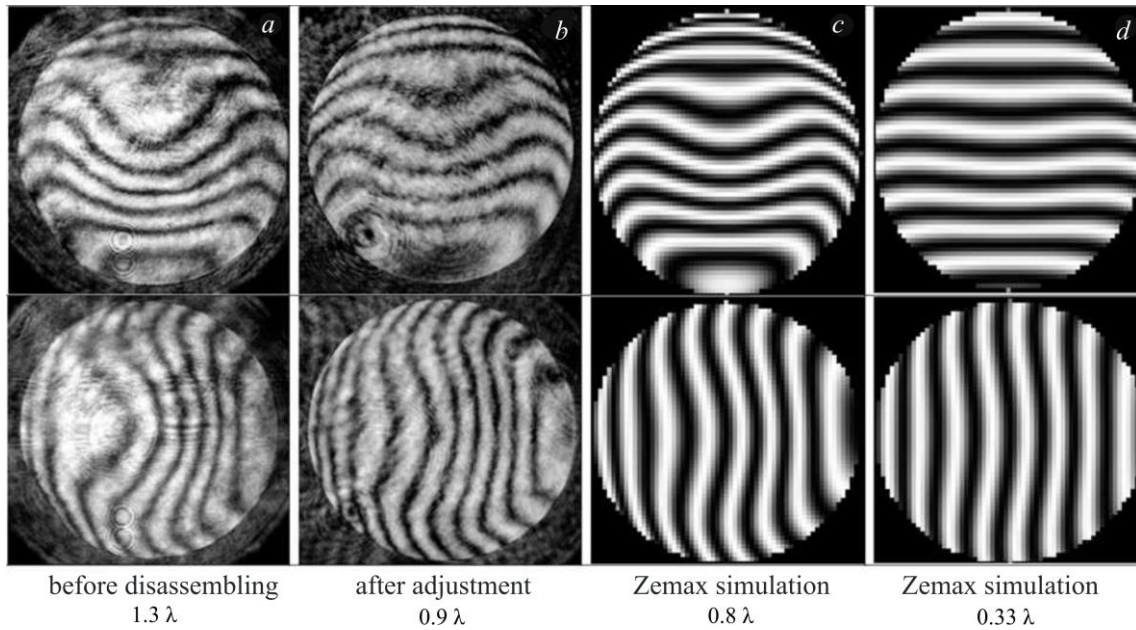


Figure 12. Wavefront of the teleobjective in the double beam path and maximum wavefront errors: λ 6328 Å (a, b, c); λ 3933 Å (d)

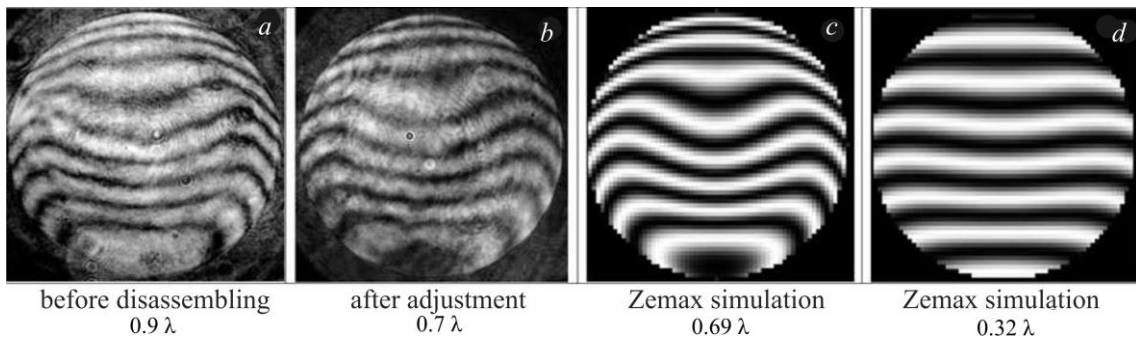


Figure 13. Teleobjective + field lens wavefront in the double beam path and maximum wavefront errors: λ 6328 Å (a, b, c); λ 3933 Å (d)

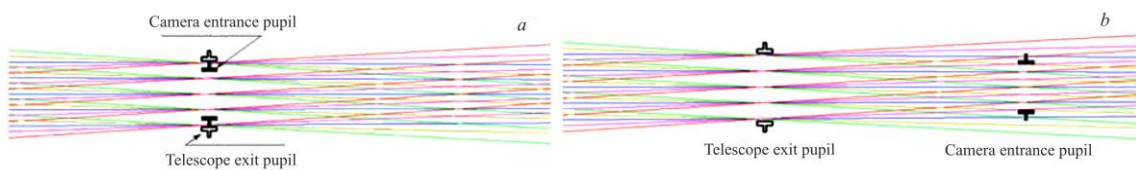


Figure 14. Dimensions and position (relative) of the exit pupil of the telescope and the entrance pupil of the camera: the pupils are aligned, the edge zone of the teleobjective does not work (a); the pupils are spaced, the irradiance from the edge zone falls into the camera, but is vignetted by its pupil (b)

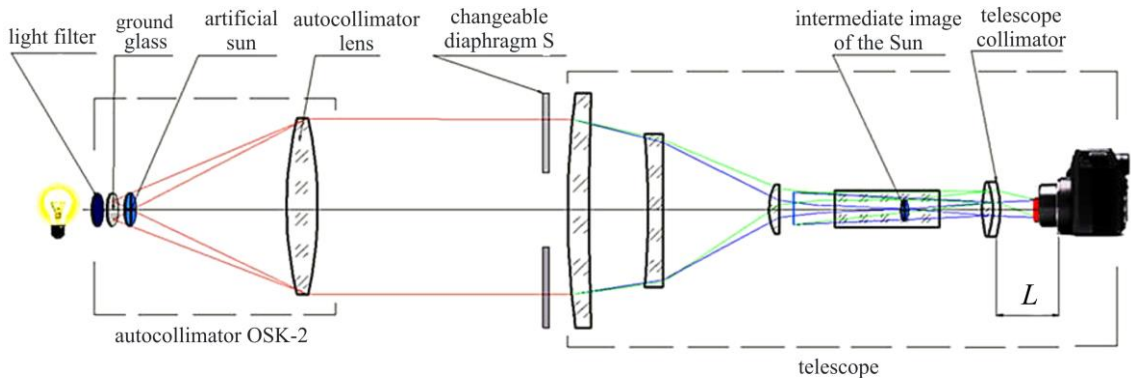


Figure 15. Installation with an artificial sun for determining alignment of the telescope and camera pupils

to leave unchanged the optical path length and reduce the Sony camera exposures instead of BF its optical equivalent — a transparent K8-glass “block” — was installed. The autocollimator illuminated only a part of the 180 mm aperture of the telescope, but the size of the exit pupil of the system (12 mm) still exceeded the calculated size of the camera’s entrance pupil (see Figure 14, *b*).

The measurement procedure was to determine the gradient of the change in the illumination of a solar image depending on a change in the illuminated area of the teleobjective (entrance pupil size) for different distances between the pupils of the telescope and camera.

The distance between the pupils was changed by moving the camera whose position L was measured from the fixed flange of the lens to the collimator of the telescope (Figure 15). The range of the camera movement from 125 to 192 mm was limited by the size of its motion block in the rear flange of the telescope tube. In each position of the camera with a step $\Delta L=10$ mm, an image of the artificial sun was taken with different diaphragms changed in the 180 mm teleobjective from a diameter of 150 mm (size of the OSK2 autocollimator lens) to 20 mm.

For all positions of the camera, we have plotted $I=f(S)$ changes in the illumination of the simulator image as function of area S of the illuminated surface of the telescope’s teleobjective (Figure 16, *a, b*) for two magnifications of the camera lens (2.1^{\times} and 3.0^{\times}), which were normally used for solar observations at the Baikal Astrophysical Observatory (BAO). The illumination I is normalized with respect to its maximum value.

Note that with increasing zoom the focus and size of the pupil of the camera lens, as well as the effective diameter of the teleobjective and image size on matrix increase. At the same time, a greater number of pixels are applied and spatial resolution becomes higher.

The behavior of curves in Figure 16 shows that when the teleobjective area decreases (when the external zone of the teleobjective, irradiance from which misses the camera pupil, is overlapped), the image illumination first remains unchanged and then decreases. This confirms that the exit pupil of the telescope is larger than the entrance pupil of the camera for 2.1^{\times} and 3.0^{\times} zooms. An “irregularity” in the behavior of the curves in Figure 16 can most likely be explained by the instability of the light source and possible imprecise centering of diaphragms when installed in the barrel of the teleobjective. The uppermost curve in Figure 16, *a, b* has the longest horizontal section (constant illumination) and a sharp dip. It corresponds to the camera position when pupils of the telescope and camera coincide in position (see Figure 14, *a*). If the pupils are spaced along the axis (see Figure 14, *b*), the illumination begins to decrease earlier. The greater the distance between the pupils, the more noticeable it is, as shown by other curves in Figure 16 *a, b*. The cause of this is the light passing through the entrance pupil from the teleobjective zones, which are farther from the center. Overlapping of this light begins earlier when diaphragms decrease. Image illumination is maximum when the pupils

are aligned. For the camera with 2.1^{\times} zoom the longest gentle slope and sharp dip of the curve are observed when $L=162$ mm; and for 3^{\times} , when $L=192$ mm. In these curves, the beginning of the dip corresponds to the diaphragm size ~ 70 – 80 mm on the teleobjective in the former case and to ~ 100 – 110 mm in the latter. The experimentally determined sizes of the entrance pupils corresponding to these diaphragms approximately correspond to the calculated sizes of the pupils of the camera — 6.2 mm for 2.1^{\times} zoom and 8.4 mm for 3^{\times} zoom. This means that the telescope employs only the 77.5 and 105 mm aperture for respective zooms. Zones outside of these diameters at aligned pupils do not work, and the theoretical resolution for the 180 mm teleobjective cannot be realized in the telescope.

The position of the camera for 3^{\times} when the pupils are aligned is by 67 mm farther from the collimator than its installation in previous years.

The camera was moved until the pupils were aligned. However, with the great difference between diameters of the telescope’s exit pupil (14.4 mm) and the camera’s entrance pupil (8.4 mm), when instead of the 180 mm lens only its 105 mm central zone operates, it is difficult to say how much a small movement of the camera along the axis affects the resolution of the telescope: mismatch of the pupils in position, on the one hand, leads to vignetting of the edge work zone, and, on the other, to an increase in the diameter of the work zone and its nonuniform illumination.

If the telescope lens is uniformly illuminated by a point source and its edge, central or other zones are not vignetted (Figure 17, *a*, line 1 at a level of 1.0), the point spread function (PSF) has the form with characteristic energy distribution — Airy pattern (Figure 17 *b*, curve 1). The angular radius of the central circle is $1.22 \lambda/D$. At the same angle, the diffraction image of a point can be projected on the celestial sphere and identify it with an imaginary object whose radius is visible for an observer at the same angle [Koronkevich, 2005].

If the transmission of the lens zones as compared to the central zone gradually decreases from 1 to 0, the central maximum of PSF expands, and diffraction rings disappear (Figure 17, *a, b*, curves 2). If the transmission of the edge zone is higher than in the center of the lens, the central maximum becomes narrower, and the intensity of rings increases (Figure 17, *a, b*, curves 3).

The described pattern corresponds to a deep modulation of the transmission of the lens zones from 0 to 1. Turning back to the chromospheric telescope, we can say that due to the fact that the telescope’s exit pupil is much larger than the camera’s entrance pupil, the slight difference in their position does not cause any noticeable change in the diffraction pattern, only reduces the amount of transmitted light, (see Figure 16, *a, b*).

In the spring of 2018, the telescope was restored to its equatorial mount at the astronomical pavilion of the Baikal Observatory and was again included in the program of the Sun Service. A solar image is taken by the Sony camera in the autofocus regime. The 3^{\times} zoom

with the collimator $f=170$ mm on the 5.3×7.1 mm matrix (1700×2000 pixels) yields a solar disk image of

diameter 2.6 mm (Figure 18). For every 1 arcsec of a solar image there is 0.43 pixel.

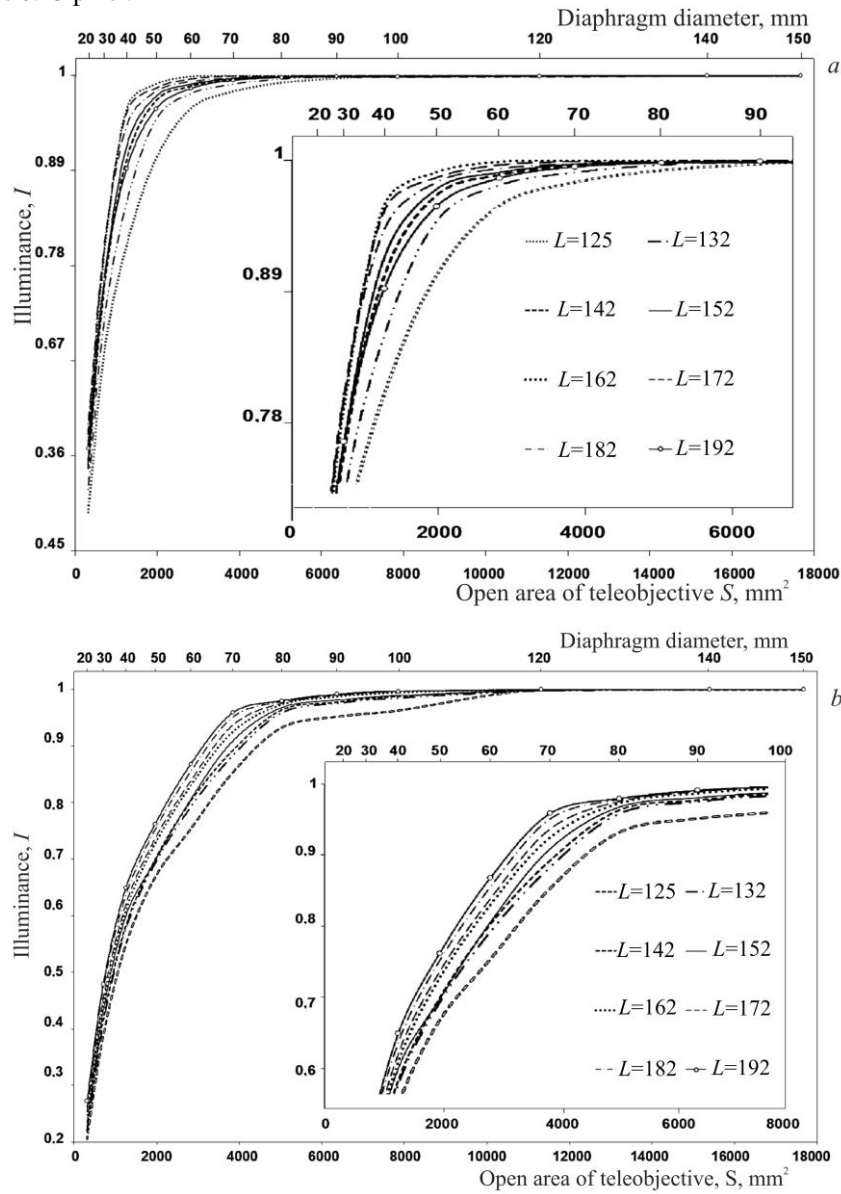


Figure 16. Panel a shows illumination of solar simulator images as a function of the open area of the teleobjective with the collimator $f=170$ mm for different camera positions L ; 2.1^{\times} zoom. The central part of the plot is enlarged (right). Panel b shows the image illumination as a function of the open area of the teleobjective with a collimator $f=170$ mm for different camera positions L ; 3^{\times} zoom

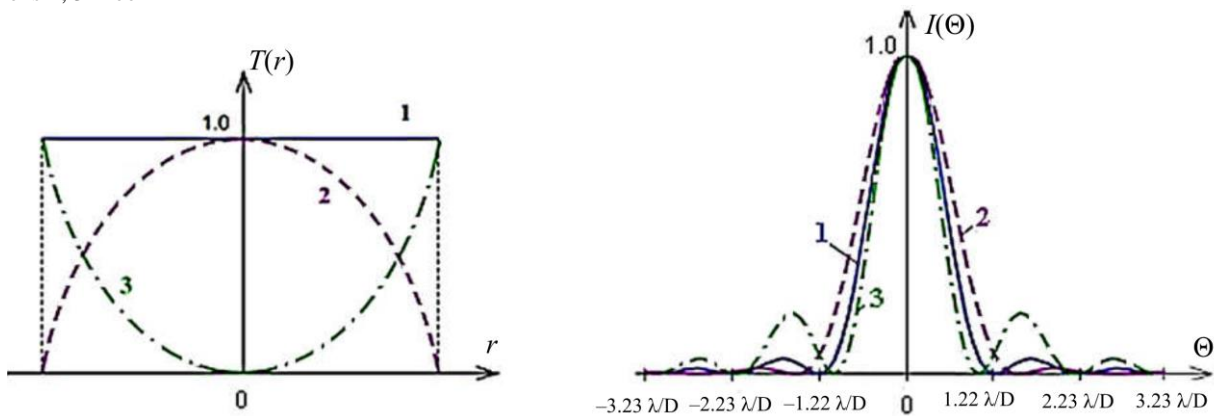


Figure 17. Point spread function versus lens transmission: transmission function $T(r)$ along the radius r of the lens (a); point spread function $I(\Theta)$, Θ is the angular coordinate of the observation point (b). Curve 1 indicates that transmission along the radius does not change; curve 2, transmission decreases toward the edge of the lens; curve 3, transmission increases toward the edge of

the lens

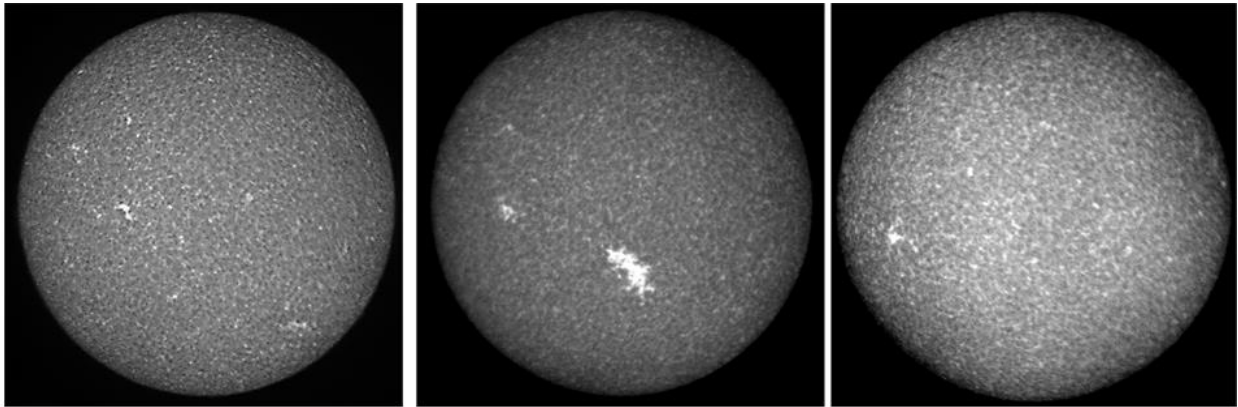


Figure 18. Solar images in the K CaII line center with collimator ($f=170$ mm) obtained on April 18, May 29, and November 28, 2018

As we can see, with the camera Sony Cyber-Shot DSC-S85 and the collimator $f=170$ mm the theoretical resolution of the telescope is not realized, therefore we have calculated two possible modernization schemes for the telescope to improve the spatial resolution.

For the Sony camera (with the known position of the entrance pupil) we calculated a new collimator with a focal length $f=89$ mm. The collimator, which was calculated taking into account the radius set of ISTEP SB RAS glasses, consists of two lenses (K8 glass) with an air gap. With the full (180 mm) aperture of the telescope, the collimator forms a 7 mm exit pupil and the entire light from the teleobjective completely passes through the entrance pupil of the Sony camera. The solar image diameter on the matrix is 4.0 mm; for every 1 arcsec there is 0.66 pixel. To work with the new collimator, it is necessary to shorten the telescope tube — to bring the flange with the camera nearer to BF by 60 mm (Figure 19, *a*).

In the second scheme (Figure 19, *b*), instead of the

Sony camera the available CCD camera Basler Ace ac2040-90um with the matrix size 11×11 mm (2000×2000 pixels) is proposed to be used. The lens ($f=90.6$ mm) that forms a 20 mm real intermediate solar image from the filter to the matrix has been designed.

The solar image size on the matrix is 8.8 mm; for every 1 arcsec there is 0.83 pixel. This scheme is an analogue of the first scheme for the K CaII telescope with formation of the 48 mm solar image on film of the 80 mm camera [Trifonov et al., 1992]. To realize this scheme, it is necessary to lengthen the telescope tube — actually to reinstall the section removed to install the camera Sony Cyber-Shot DSC-S85 in 2003 [Trifonov et al. 2004].

Unfortunately, with the available camera and CCD matrix we cannot realize the theoretical resolution of the telescope — take a full solar disk image of the solar chromosphere in the K CaII line with a spatial resolution of less than 1".

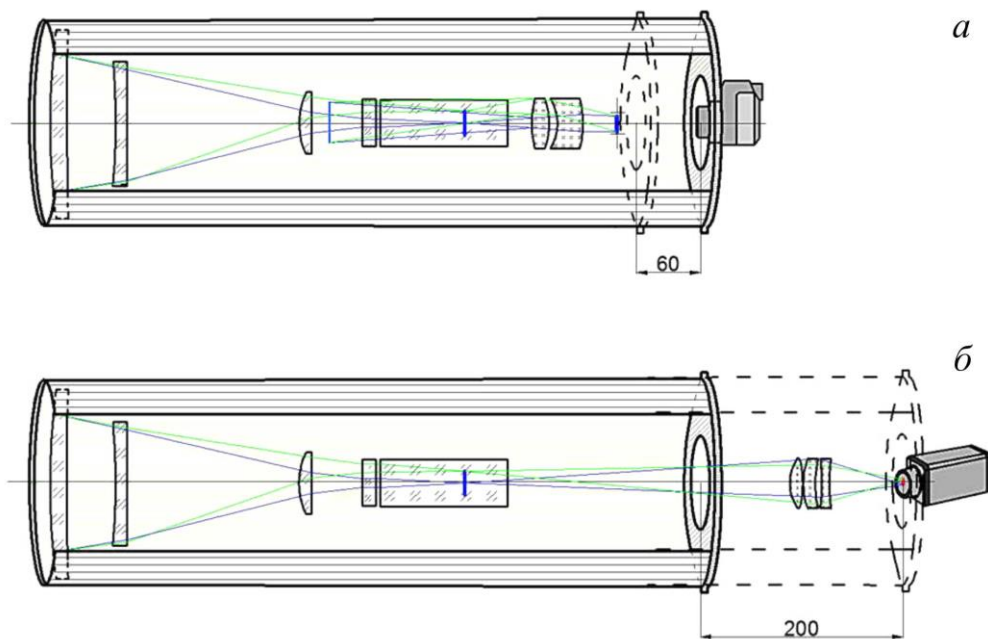


Figure 19. Optical scheme for the K CaII telescope: with the new two-lens collimator for Sony camera (*a*); with the new three-lens objective reimaging a solar image for CCD camera (*b*)

CONCLUSION

The full-disk chromospheric telescope in the K CaII line has again been included in the programs of Sun Service and scientific research. All optics of the telescope has been cleaned and readjusted. The resulting wavefront interferograms of the teleobjective and telescope show that distortions of the wavefront of the entire optical path are within 0.25λ . The out-of-operation UV polarizers have been replaced, and passbands of tunable BF stages have been adjusted. Spectral characteristics of BF and prefilter provide a sufficiently high contrast of monochromatic images of large-scale phenomena.

In recent years, most results of studies of the solar chromosphere in the H and K CaII lines have been obtained from filter observations. Such observations have a serious limitation imposed by filter passband. Modern observations in calcium lines place higher demands not only on the spatial resolution of the telescope, but also on the width and spectral finesse of the filter passband. The problem is that the contribution of the chromosphere in the H and K CaII lines is limited by narrow line cores less than 0.2 \AA wide [Reardon et al., 2009]. The most advanced calcium filters have $\sim 0.3 \text{ \AA}$ FWHM. But even such observations are not suitable for the study of the chromosphere because they contain information about a large layer of the solar atmosphere — from the photosphere to the chromosphere.

In this regard, we plan to reduce the BF passband for the K CaII line to 0.2 \AA . The calculations have shown that it is necessary to set up a new CCD camera with a large matrix to obtain images with resolution less than 1 arcsec.

We thank V.M. Grigoryev for scientific advice and support of this work; head of BAO A.V. Borovik and BAO staff members A.A. Zhdanov, A.V. Ovcharov as enthusiasts of observations at chromospheric telescopes.

The work was performed with budgetary funding of Basic Research program II.16. The results were obtained using the Unique Research Facility Large Solar Vacuum Telescope [<http://ckp-rf.ru/usu/200615>].

REFERENCES

- Evans J.W. The birefringent filter. *J. Opt. Soc. Am.* 1949, vol. 39, pp. 229–242. DOI: [10.1063/1.3066514](https://doi.org/10.1063/1.3066514).
- Issledovanie vozmozhnosti uvelicheniya propuskaniya polarizatsionnykh filtrov dlya vidimoi oblasti spektra, ispol'zuemykh v IPF* [Studying the possibility of transmittance increase for polarization filters in visible spectral region used in IBF]. Report SOI, LOMO. 1984, 59 p. (In Russian).
- Klevtsov Yu.A. Features of operation of birefringent filter in telescope optical scheme *Issledovaniya po geomagnetizmu, aeronomii i fizike Solntsa* [Res. on Geomagnetism, Aeronomy and Solar Phys.]. 1984, no. 69, pp. 183–189. (In Russian).
- Koronkevich V.P. *Formirovanie izobrazheniya v opticheskikh sistemakh* [Image formation in optical systems]. Tutorial. Novosibirsk, 2005. NsTU Publ., 76 p. (In Russian).
- Reardon K.P., Uitenbroek H., Cauzzi G. The solar chromosphere at high resolution with IBIS. III. Comparison of CaII K and CaII 854.2 nm imaging // *Astron. Astrophys.* 2009, vol. 500, iss. 3, pp. 1239–1247. DOI: [10.1051/0004-6361/200811223](https://doi.org/10.1051/0004-6361/200811223).

Skomorovsky V.I., Kushtal G.I., Lopteva L.S., Proshin V.A., Trifonov V.D., Chuprakov S.A., Khimich V.A. Chromospheric telescope of Baikal Astrophysical Observatory. New light. *Solar Terr. Phys.* 2016, vol. 2, iss. 2, pp. 82–103. DOI: [10.12737/17376](https://doi.org/10.12737/17376).

Sotnikova R.T. Simultaneous observations of solar chromosphere in H α and K CaII lines *Solnechnye dannye* [Solar Data]. 1977, no. 12, pp. 97–100. (In Russian).

Trifonov V.D., Skomorovsky V.I., Pipin V.V., Domyshv G.N., Grigoryev V.M. Chromospheric K CaII telescope. *Issledovaniya po geomagnetizmu, aeronomii i fizike Solntsa* [Res. on Geomagnetism, Aeronomy and Solar Phys.]. 1992, iss. 99, pp. 128–149. (In Russian).

Trifonov V.D., Golovko A.A. Skomorovsky V.I. Chromospheric observations at Baikal Astrophysical Observatory using CCD cameras. *Solnechno-zemnaya fizika* [Solar-Terr. Phys.]. 2004, iss 6, pp. 178–180. (In Russian).

URL: <http://ckp-rf.ru/usu/200615> (accessed February 6, 2019).

How to cite this article

Lopteva L.S., Kushtal G.I., Proshin V.A., Skomorovsky V.I., Firstov S.V., Khimich V.A., Chuprakov S.A. Chromospheric K CaII telescope of Baikal Astrophysical Observatory. New light. *Solar-terrestrial physics.* 2019. Vol. 5. Iss. 2. P. 116–128. DOI: [10.12737/stp-52201917](https://doi.org/10.12737/stp-52201917).